COR1-A Final Assembly Tests May 2004

William Thompson
June 2, 2004

This is a report on the result of the measurements made of the COR-1A instrument as part of the final assembly procedure, during May 2004 in the COR-1 clean room facility in Building 5.

1 Focus

To measure the instrument resolution, an Air Force 1951 resolution test target was placed at the eyepiece location of a Meade telescope. To take the difference between nitrogen and vacuum focus into account, the target was moved back by a measured distance from the Meade's infinity focus.

Measurements were made at the following six locations on the detector, relative to the center of the CCD:

Location	X (mm)	Y (mm)
A	0	7.1
B	0	10.3
C	-5	-5
D	5	-5
E	-9	-9
F	9	-9

At each of the above points, measurements were made at 5 focus positions on the Meade telescope, centered around the nominal position of 8.42 mm, and at ±1.5 mm and ±3 mm. Because of vignetting problems, points A and B were done with the Meade telescope at one location, and the rest of the points were done with another location of the Meade telescope. Also, because of vignetting, the original B location of 12.7 mm could not be obtained.

Figure 1 shows a sample Air Force Target image, taken at full 13.5×13.5 μm resolution. Group 4-4 corresponds to the Nyquist frequency, while 3-4 would be the Nyquist frequency for 2×2 binning.

To characterize the data, the contrast of group 4-1 was analyzed. This group has bars which are very close to 1.5 pixels wide. The results are shown in Figure 2. No dependence was found on polarizer position.

2 Polarization angle

To calibrate the angle of the polarizer, the instrument was exposed to diffuse light polarized vertically, and then by light polarized horizontally. For each, the procedure STEP15 was run, to measure the response stepping every 15°. The results are shown in Figure 3. Fitting the function

$$y = A\cos^2(\phi - \phi_0) + B$$

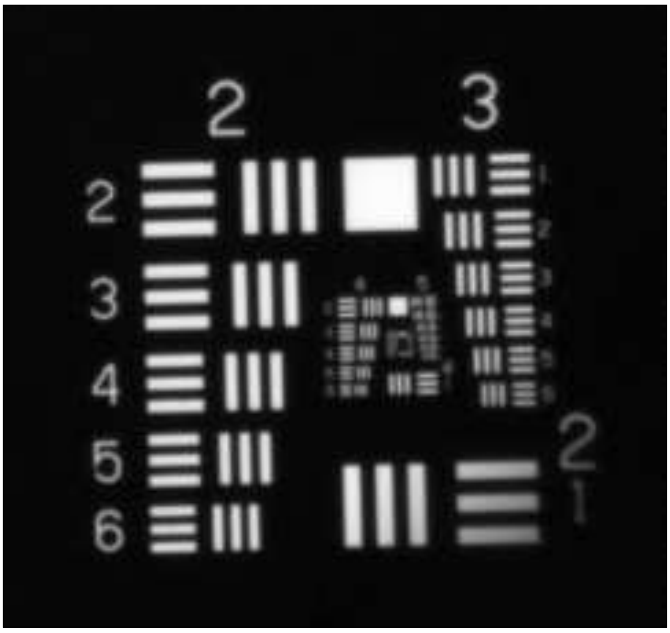

Figure 1: Sample image of Air Force 1951 resolution test target. This image has been rotated by 90° and reflected to make the lettering more readable.

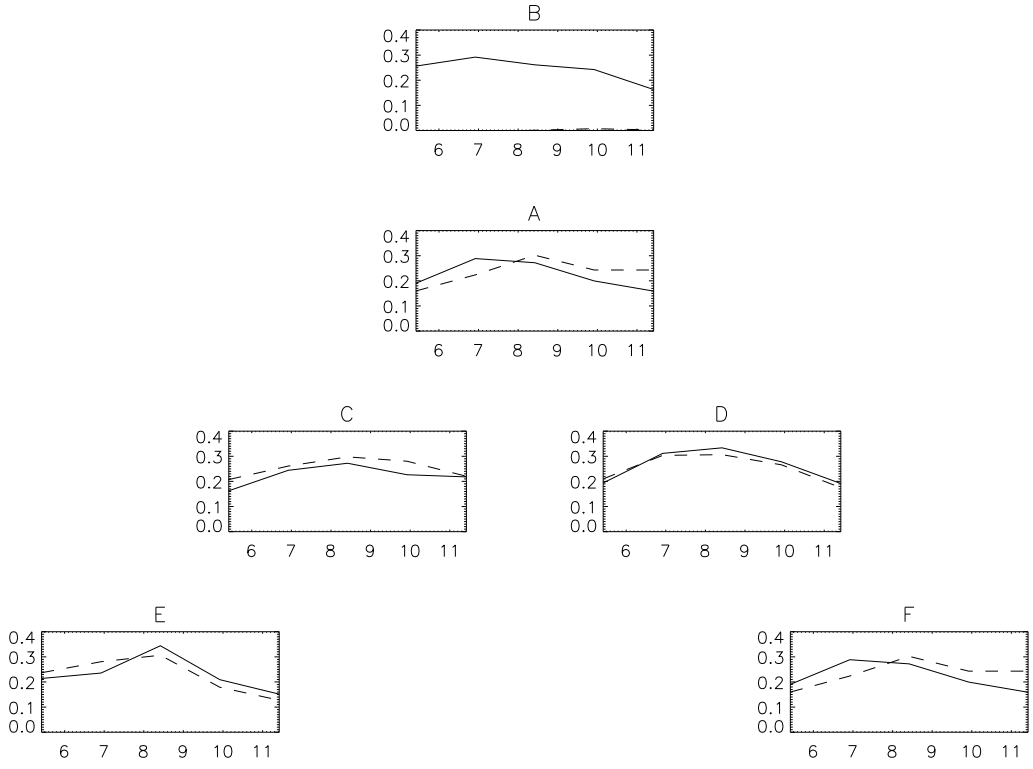

Figure 2: Contrast values as a function of Meade focus for several positions on the detector. Solid lines are for vertical bars, dashed for horizontal bars.

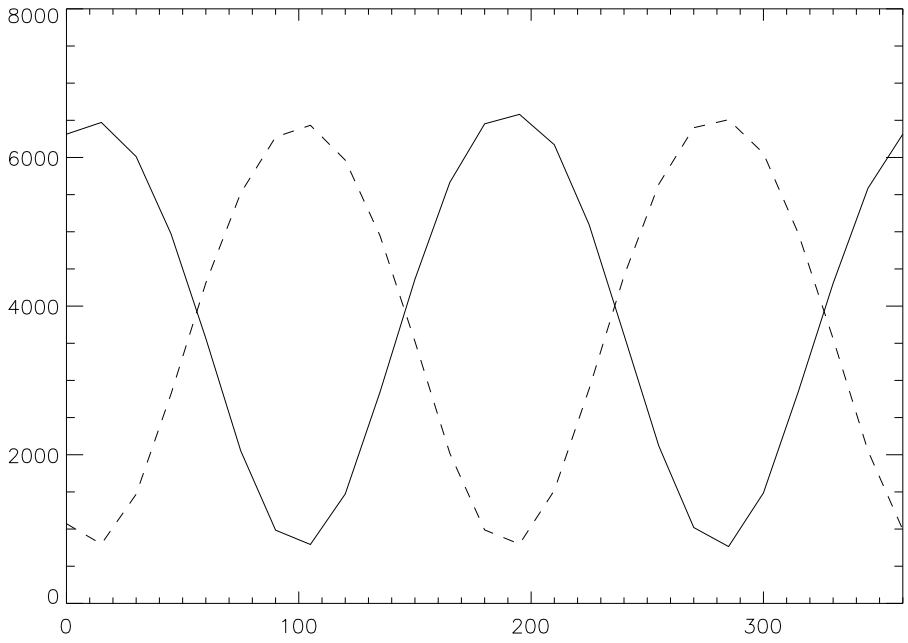

Figure 3: Relative response of the instrument as a function of polarizer angle to light polarized vertically (solid line), and horizontally (dashed line).

to these curves gives an offset of 11.27 ± 0.40 and 10.83 ± 0.38 degrees respectively. Averaging these two results together gives 11.04 ± 0.28 degrees. This corresponds to 4.4 ± 0.1 steps of the hollow core motor.

Note that the curves in Figure 3 do not go all the way to zero. This is because the amount of dark current in the images that use the shutter is higher than for those that don't. The reason for this is because of the extra delay involved in sending the commands to the shutter mechanism. Most of the delay comes from creating windows on the GSE computer to display each command as it's executed.

3 Polarizer wedge

Measurements of the Air Force resolution target, made every 15°, can be used to derive the amount of image motion as a function of polarizer position. The results are shown in Figure 4. This test shows that the target image makes a small circular motion with a radius of 0.19 pixels (2.5 μm, 0.7 arcsec), and a phase angle of 173.°6. A separate test gives a radius of 0.27 pixels (3.6 μm, 1.0 arcsec), and a phase angle of 170.°5.

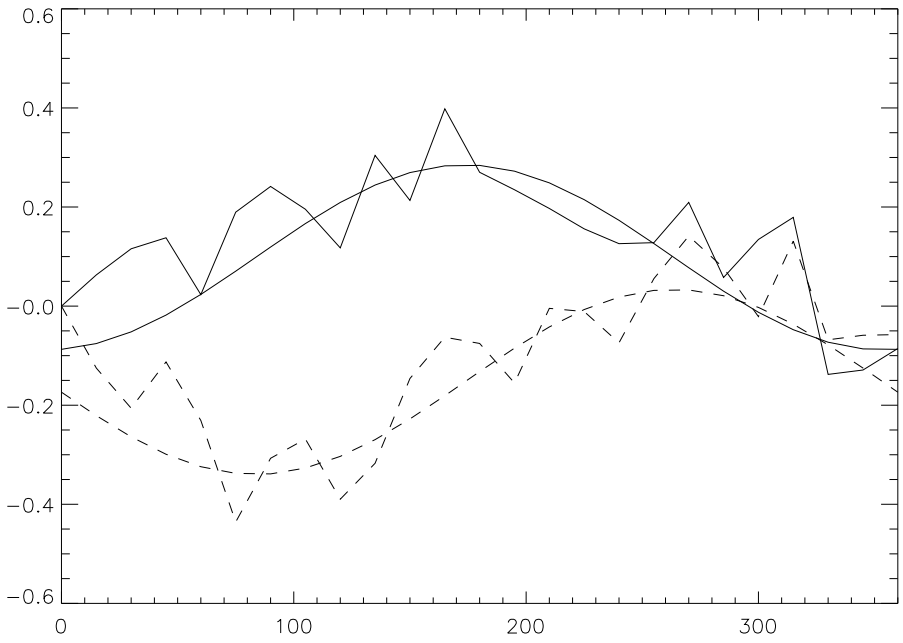

Figure 4: Target position as a function of polarizer angle, relative to the position at 0°, in the X (solid) and Y (dashed) directions. Also shown are the curves representing the fitted circle.

4 Focal plane mask

Two measurements were made of the focal plane mask, using the NRL "Sun bucket" to mimic the solar illumination. It turned out that the first measurement run, on May 14, was made with a too-small focal plane mask, allowing part of one of the rings to make it through. The mask was modified, and more measurements were made on May 25. Figure 5 compares the images from the two measurement runs. Figure 6 shows vertical traces through these images.

From these data, one can make the following conclusions:

- The narrow bright ring segment seen in the May 14 data has been successfully removed from the May 25 data. However, there's a broad outer ring which persists.
- The boundaries of the broad ring appear to coincide with the penumbra boundaries of the focal plane mask.
- Both data sets show non-negligable background levels within the shadow of the focal plane mask. Separate tests have shown that this background level is independent of the lamp, and is probably caused by a light leak somewhere in the instrument. The area outside the mask shadow is also affected by ambient light within the machine shop area, which was probably different for the two tests.

A Gamma Scientific photometer was used to cross-calibrate the "Sun bucket" against the Sun. An Andover bandpass filter from the ETU, centered at 700 nm with a FWHM of 80 nm, was placed

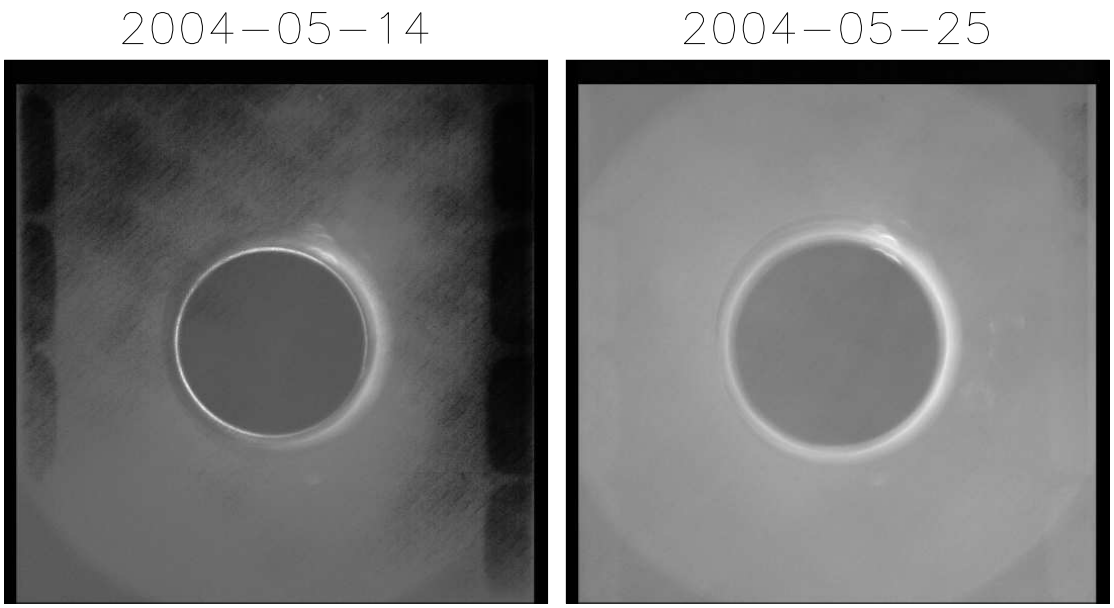

Figure 5: Focal plane mask measurements from runs on May 14 and May 25, with different sized focal plane masks.

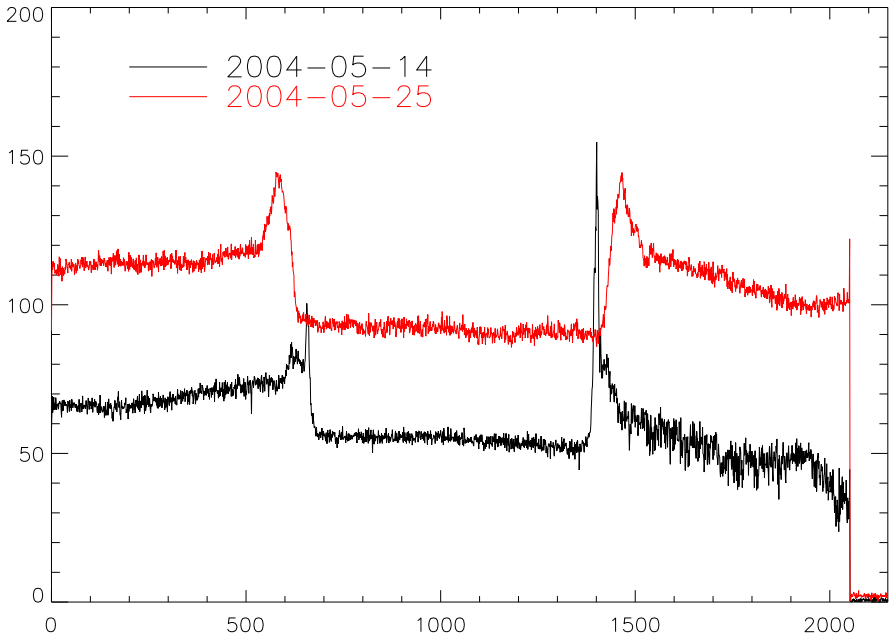

Figure 6: Vertical traces through the images of Figure 5, in DN/sec.

over the photometer sensor. The photometer was placed in lambda mode at 700 nm, with units of W/cm^2 selected. The "Sun bucket" was measured at 5.4×10^{-5} W/cm^2, while the Sun itself was measured at 1.5×10^{-2} W/cm^2. Thus, the "Sun bucket" is 0.36% of a solar brightness. Assuming that the true baseline is given by the area under the mask shadow, the ring would saturate between 0.3–0.5 seconds, while the area outside the ring could be exposed for 2 seconds before saturating.

If we take the irradiance of 5.4×10^{-5} W/cm^2, and convert it into signal at the detector, we get approximately 5×10^7 DN/sec. This is based on the following factors:

- $\tau = 0.9082$ is the transmission of the various optical elements.
- $A = 6.566$ cm^2 is the effective area.
- Each pixel is 3.75 arcsec^2.
- A "Sun" with the same irradiance would be 960 arcsec in radius. This allows us to convert the irradiance into a radiance.
- The ratio of the throughput of the flight filter to the ETU bandpass filter is ∼0.3.
- The Q.E. of the CCD is ∼0.8.
- The digitization is 15 electrons per data number (DN).

Thus, a rate of 50–100 DN/sec, as implied by Figures 5 and 6, is about 1–2 $\times 10^{-6}$ $B/B_\odot$. This is only a rough estimate, but it does indicate that we're close to where we need to be. The specification for the maximum ring brightness is 3×10^{-6} $B/B_\odot$.

5 Flat field

To measure the flat field, a bright, diffuse light source was placed directly in front of the diffuser window in the COR-1 door. The results are shown in Figure 7. There are some faint scattered light features which are probably caused by the high amount of considerably off-axis light coming from the diffuser window. The most prominent is a spot in the center of the occulter shadow, which is about 10–15% of the unvignetted area. This feature has been seen before in flat-field images from the ETU, but not in images where the instrument was exposed to more solar-like collimated light.

Much fainter is a streak of scattered light moving radially outward from the center spot, which rotates in synchronization with the polarizer mechanism. This introduces a variation of ∼1% for the flat field in the unvignetted area.

6 Exposure time test

The procedure EXPTIMETEST takes a series of exposures ranging from 0.1 to 10 seconds, together with the associated dark images. Intercomparing the resulting images allows the accuracy of the exposure times to be explored. To keep the instrument from saturating at the longer exposure times, the lamp current was reduced from 6 to 4 amps. Even so, some saturation occured at the longest exposure times due to dark current in the room temperature CCD.

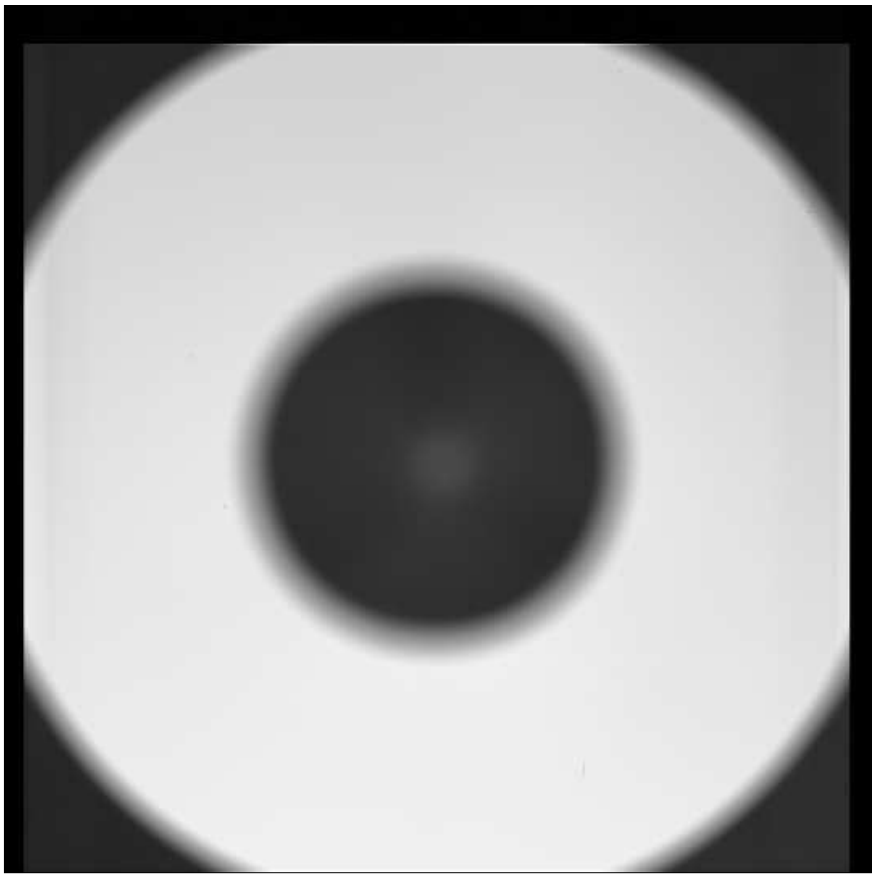

Figure 7: Instrument flat field.

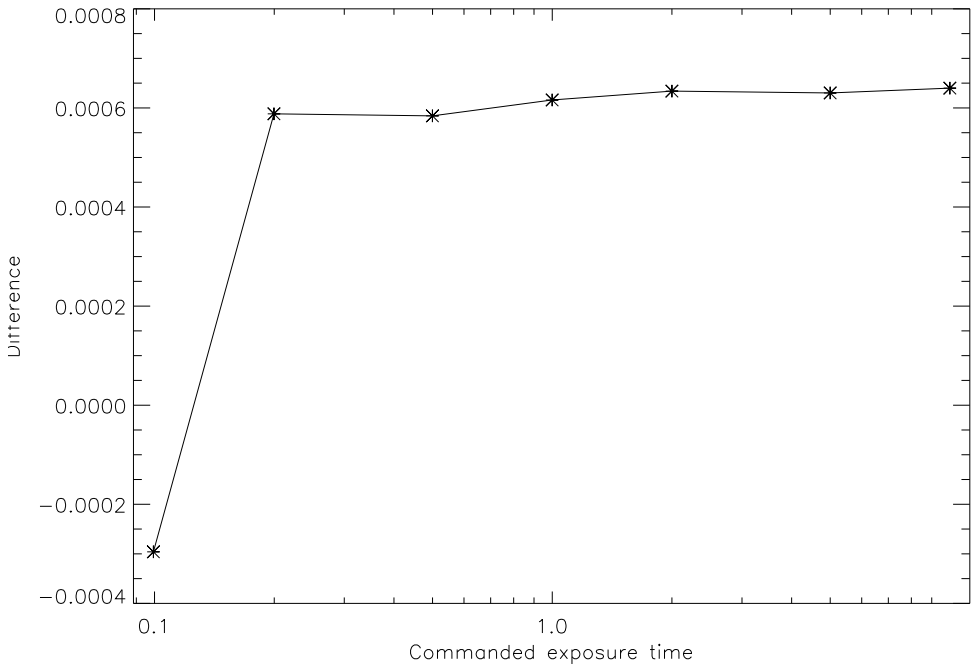

Figure 8: Difference between measured and commanded exposure times.

Two keywords in the FITS headers are related to the exposure times. The keyword EXPCMD contains the commanded exposure time, while EXPTIME contains the measured exposure time, based on the motion of the shutter mechanism. For dark images, EXPTIME is calculated using a different algorithm, and is not reliable. Figure 8 shows the difference between the measured and commanded exposure times. For most exposure times, the measured exposure exceeds the command exposure by ∼0.6 milliseconds. The only exception is for a commanded exposure time of 0.1 seconds, where the measured exposure time was 0.3 milliseconds shorter. (These results should not be confused with repeatablility, which was not addressed by this test—see Section 7.)

Figure 9 shows the relationship between the exposure time and the measured signal in the detector. The signal was derived by subtracting the average signal in the complete shadowed areas of the detector from that in the completely unshadowed area. The associated dark image was subtracted from each image before processing. From 0.1 to 2 seconds, the instrument behaves linearly. After that, the instrument starts to saturate, mostly due to thermal noise from the room temperature CCD. A straight line fit to the first five points is also shown. The fit doesn't go quite through the origin, which may be because of the differences in dark current between shuttered and unshuttered exposures (see Section 2), or because the lamp wasn't completely steady.

7 Exposure repeatability

The primary testing of exposure repeatability was performed on the shutter mechanism before it was delivered to the COR-1 team. However, some information on repeatability can be gleaned from the EXPTIME values in the various FITS headers. To explore the question of exposure repeatability, the exposure times were read in from all the runs of the sequence PBSERIES. Figure 10 shows the

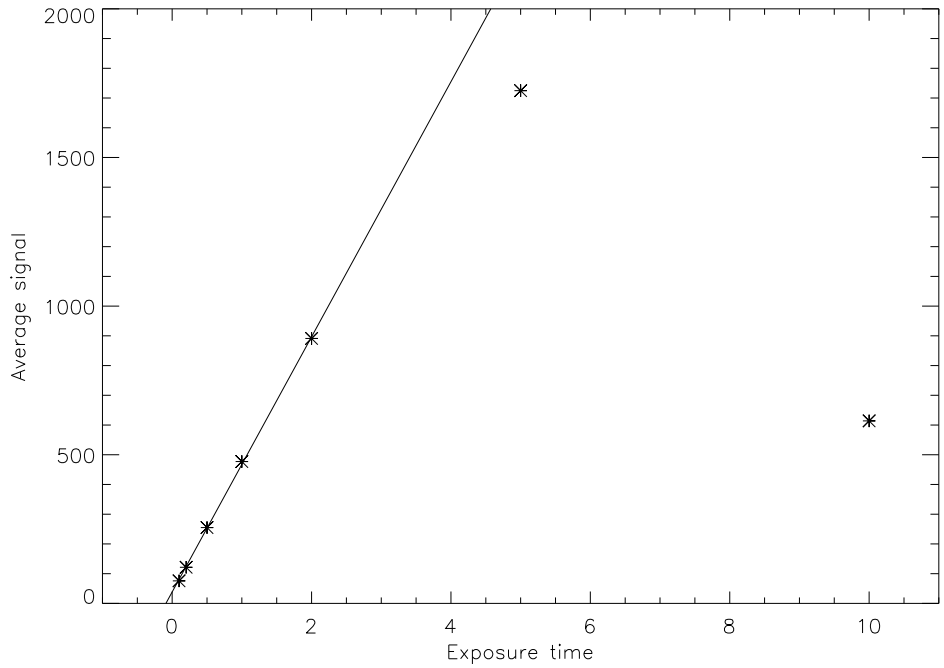

Figure 9: Comparison between measured signal and exposure time. The exposure times above 2 seconds are affected by saturation in the detector.

standard deviations from each sequence of three images, plotted against the exposure time. The exposure times are highly repeatable.

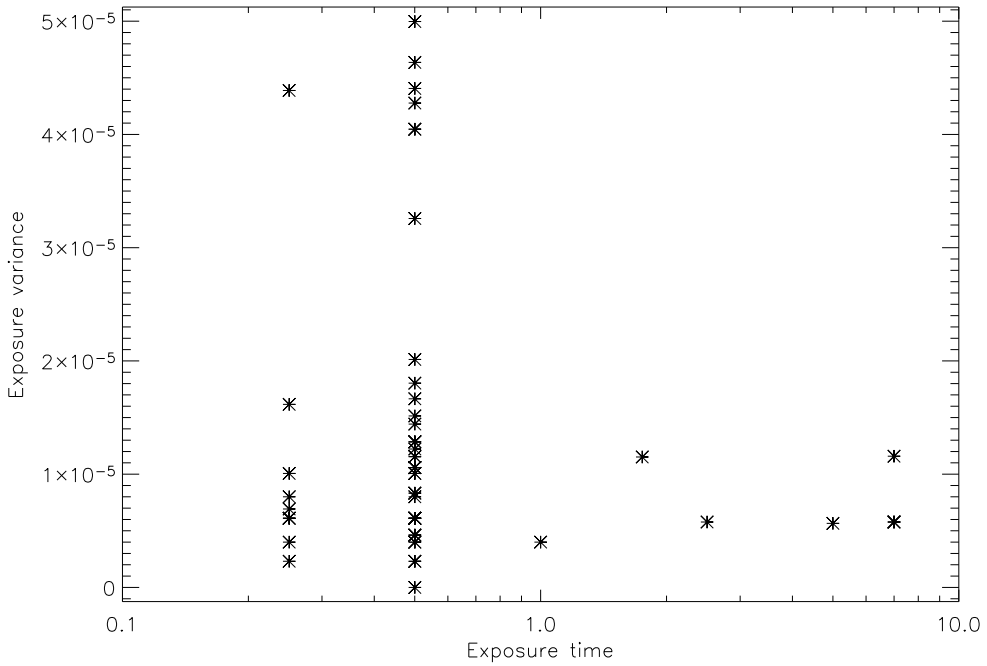

Figure 10: The RMS deviation of exposure times for each run of PBSERIES, plotted against the average exposure time.